Development 134, 691-702 (2007) doi:10.1242/dev.02767

SEL-2, the *C. elegans* neurobeachin/LRBA homolog, is a negative regulator of *lin-12/Notch* activity and affects endosomal traffic in polarized epithelial cells

Natalie de Souza[1], Laura G. Vallier[1,2], Hanna Fares[1,3] and Iva Greenwald[1,*]

The vulval precursor cells (VPCs) of *Caenorhabditis elegans* are polarized epithelial cells that adopt a precise pattern of fates through regulated activity of basolateral LET-23/EGF receptor and apical LIN-12/Notch. During VPC patterning, there is reciprocal modulation of endocytosis and trafficking of both LET-23 and LIN-12. We identified *sel-2* as a negative regulator of *lin-12/Notch* activity in the VPCs, and found that SEL-2 is the homolog of two closely related human proteins, neurobeachin (also known as BCL8B) and LPS-responsive, beige-like anchor protein (LRBA). SEL-2, neurobeachin and LRBA belong to a distinct subfamily of BEACH-WD40 domain-containing proteins. Loss of *sel-2* activity leads to basolateral mislocalization and increased accumulation of LIN-12 in VPCs in which LET-23 is not active, and to impaired downregulation of basolateral LET-23 in VPCs in which LIN-12 is active. Downregulation of apical LIN-12 in the VPC in which LET-23 is active is not affected. In addition, in *sel-2* mutants, the polarized cells of the intestinal epithelium display an aberrant accumulation of the lipophilic dye FM4-64 when the dye is presented to the basolateral surface. Our observations indicate that SEL-2/neurobeachin/LRBA is involved in endosomal traffic and may be involved in efficient delivery of cell surface proteins to the lysosome. Our results also suggest that *sel-2* activity may contribute to the appropriate steady-state level of LIN-12 or to trafficking events that affect receptor activation.

KEY WORDS: LIN-12, Notch, BEACH, Endocytosis, *Caenorhabditis elegans*

INTRODUCTION

Regulated endocytic trafficking of receptors is emerging as an important way to control receptor activity. Endocytosis of ligand-activated receptors can serve as a mechanism for either attenuating or enhancing signaling (Gonzalez-Gaitan, 2003; Miaczynska et al., 2004; Le Roy and Wrana, 2005). Endocytic traffic of non-activated receptors plays a part in controlling their steady-state level and can thereby affect the sensitivity of cells to ligands. Mutations that alter this process can have profound phenotypic effects. For example, defects in multivesicular endosome sorting can cause inappropriate activation of LIN-12/Notch, leading to cell fate change (Shaye and Greenwald, 2005) or neoplastic transformation and ectopic mitogenic signal production (Moberg et al., 2005; Thompson et al., 2005; Vaccari and Bilder, 2005; Herz et al., 2006) in vivo. In the case of the epidermal growth factor receptor (EGFR), endocytic traffic is required both for attenuation of receptor activity (Sorkin and Waters, 1993) as well as for full activation (Burke et al., 2001; Vieira et al., 1996).

LIN-12/Notch and EGFR (LET-23) regulate cell fate specification in the developing *Caenorhabditis elegans* vulva (Greenwald, 2005; Sundaram, 2006). Initially, six vulval precursor cells (VPCs), P3.p-P8.p, each have the potential to adopt fates called '1°', '2°' and '3°'. The 1° and 2° fates are vulval, meaning that they divide to produce cells that form the mature vulva, whereas the 3° fate is non-vulval. An EGF-like inductive signal from the anchor cell in the overlying gonad is followed by a LIN-12/Notch-mediated lateral signal between P6.p and its neighbors, P5.p and P7.p. As a result of inductive and lateral signaling, P3.p-P8.p take on an invariant pattern of 3°-3°-2°-1°-2°-3° fates. Mutations that affect LIN-12/Notch or LET-23/EGFR activity alter this cell fate pattern, resulting in profound phenotypic consequences that have enabled the genetic identification of core components and modulators of the signal transduction pathways.

The VPCs are polarized epithelial cells, with distinct apical and basolateral domains delineated by circumferential adherens junctions (Kim, 1997). LIN-12/Notch and LET-23/EGFR are type I transmembrane proteins that are initially present on the surface of all six VPCs; LIN-12 is present on the apical surface (Levitan and Greenwald, 1998; Shaye and Greenwald, 2002), whereas LET-23 is present basolaterally (Kaech et al., 1998; Whitfield et al., 1999). During the patterning of the VPCs, there appears to be reciprocal modulation of endocytosis and trafficking of both LET-23 and LIN-12. LET-23 is activated maximally in P6.p, leading to LIN-12 internalization via endocytosis and degradation via multivesicular endosomes (Shaye and Greenwald, 2002; Shaye and Greenwald, 2005), as well as to the production of ligands that activate LIN-12 in the neighboring cells, P5.p and P7.p (Chen and Greenwald, 2004). When LIN-12 is activated in P5.p and P7.p, LET-23 is downregulated (Whitfield et al., 1999; Stetak et al., 2006). LIN-12 target genes include factors that may negatively regulate LET-23/EGFR activity by promoting its endocytosis and degradation (Yoo et al., 2004; Yoo and Greenwald, 2005).

In this study we report the characterization of *sel-2*, identified as a negative regulator of *lin-12* activity in the VPCs. We show that SEL-2 is the single *C. elegans* homolog of two closely related human proteins, neurobeachin (also referred to as BCL8B) and LRBA (also referred to as BGL or CDC4L) (Wang et al., 2000b; Wang et al., 2001; Dyomin et al., 2002). Neurobeachin is expressed most strongly in the nervous system in mouse and human, whereas

[1]Department of Biochemistry and Molecular Biophysics, Howard Hughes Medical Institute, 701 W. 168th Street, Hammer Health Sciences, New York, NY 10032, USA. [2]Department of Biology, Hofstra University, Gittleson Hall Room 103, Hempstead, NY 11549, USA. [3]Department of Molecular and Cellular Biology, University of Arizona, Life Sciences South, Room 531, 1007 E. Lowell Street, Tucson, AZ 85721, USA.

*Author for correspondence (e-mail: dev.gree@cancercenter.columbia.edu)

Accepted 30 November 2006

LRBA is broadly expressed (Wang et al., 2000b; Dyomin et al., 2002). In humans, the neurobeachin locus has been linked to an idiopathic case of non-familial autism (Castermans et al., 2003) and spans a common fragile site on chromosome 13 (Savelyeva et al., 2006); mice lacking neurobeachin die at birth because of a lack of evoked neuromuscular transmission and a consequent inability to breathe (Su et al., 2004). LRBA is upregulated in a number of human tumor cell lines; it has been shown to lower the sensitivity of cells to apoptosis and to positively regulate the activity of the EGF receptor in tissue culture (Wang et al., 2004). In *Drosophila*, mutations in the single neurobeachin/LRBA homolog *rugose* (also referred to as DAKAP550) cause defects in eye development consistent with abnormalities in Notch and EGFR signaling (Schreiber et al., 2002; Shamloula et al., 2002; Wech and Nagel, 2005), but the basis for these defects is unclear.

Here, we have investigated the function of SEL-2/neurobeachin/LRBA on LET-23 and LIN-12 accumulation and subcellular localization, and other aspects of endocytic trafficking in polarized epithelial cells. Our observations suggest that SEL-2/neurobeachin/LRBA is involved in endosomal traffic and perhaps in efficient delivery of cell surface proteins to the lysosome in polarized cells, and may thereby potentiate *lin-12* activity in the VPCs.

MATERIALS AND METHODS

General methods

Unless otherwise mentioned, strains were maintained and experiments conducted at 20°C. The wild-type parent for all experiments was *C. elegans* var. Bristol N2 except for SNP mapping, which utilized a hybrid strain that carries sequences from Hawaiian strain CB4856 between *daf-2* and *dpy-17* on chromosome III in an otherwise Bristol background.

Alleles: LG III–*daf-2(e1370)*, *dpy-17(e164)*, *sel-2(ar219, n655)*, *lin-12(n302, n676, n379)*, *mab-21(bx53)*, *emb-5(hc61)*, *unc-79(e1068)*, *pha-1(e2123)*; LG V–*sel-10(ar41)*, *him-5(e1490)*; LG X–*rme-6(b1018)*. Information about these alleles may be obtained via Wormbase at http://www.wormbase.org.

Transgenes: *arIs41[lin-12::gfp]* expresses LIN-12::GFP under the control of *lin-12* regulatory sequences (Levitan and Greenwald, 1998); LIN-12::GFP is visualized by antibody staining. *zcIs4[hsp-4p::gfp]* is a marker for ER stress (Urano et al., 2002). *arIs92[egl-17p::cfp-lacZ]* may be used as a marker for the VPC 2° fate by assessing descendants at the L4 stage (Burdine et al., 1998; Inoue et al., 2002). *arIs12[lin-12(intra)]* expresses the intracellular domain of LIN-12 under the control of *lin-12* regulatory sequences (Struhl et al., 1993). *arEx551* and *arEx562* are extrachromosomal arrays carrying a PCR fragment spanning the *sel-2(+)* genomic region. *arEx545* and *arEx546* are extrachromosomal arrays carrying PCR fragments encoding SEL-2::GFP (see below). *arEx553* and *arEx554* are extrachromosomal arrays carrying LIN-12::GFP with a basolateral targeting sequence at the carboxy terminus [LIN-12::GFP-BL].

Mutagenesis, mapping and molecular identification

sel-2(*n655*) was identified after EMS mutagenesis of the weak hypermorph *lin-12*(*n302*) and initially mapped to the *mab-21–emb-5* interval (data not shown). Then, *sel-2*(*n655*) *lin-12*(*n302*)*; him-5*(*e1490*) males were crossed to hermaphrodites of a hybrid strain carrying sequences from Hawaiian CB4856 between *daf-2* and *dpy-17*, and Daf non-Dpy animals were picked in the F2 generation. Daf non-Dpy worms that retained *sel-2*(+) were examined for the presence of SNP F10f2. Fourteen out of 16 such recombinants kept SNP F10f2 but two out of 16 lost it, thus placing *sel-2* to the left of SNP F10f2 and narrowing the genomic interval containing *sel-2* to a region with four predicted genes. Sequence analysis of *sel-2*(*n655*) identified a nonsense mutation (W1012stop) in exon 12 of the gene F10F2.1.

sel-2(*ar219*) was identified in a non-complementation screen: EMS-mutagenized *dpy-17*(*e164*) hermaphrodites were crossed with *sel-2*(*n655*) *lin-12*(*n302*)*; him-5*(*e1490*) males, and an F1 Muv hermaphrodite segregated *sel-2*(*ar219*), associated with a nonsense mutation (Q330stop) in exon 8 of F10F2.1.

Sequence analysis and phylogenetic trees

The carboxy terminal region (extending from the BEACH domain to the end of the protein) of three *C. elegans* BEACH-WD40 proteins (SEL-2, VT23B5.2 and T01H10.8) and their homologs in human, mouse, *Drosophila*, and *Dictyostelium* were aligned using ClustalW (Chenna et al., 2003) and T-Coffee (Notredame et al., 2000), and maximum parsimony phylogenetic trees were found via heuristic search with PAUP version 4.0 beta 10 (Swofford, 2003). Trees were visualized with TreeView version 1.6.6 (Page, 1996). Robustness of the partitions was assessed by constructing a bootstrap consensus tree with 100 replicates.

Reporters and extrachromosomal arrays

Unless otherwise stated, all injection mixes included the *pha-1*(+) gene (50 ng/μl) and were injected into *pha-1*(*e2123*) hermaphrodites. Injected animals generated F1 progeny at 15°C for 4-5 days, and the plates were then shifted to the restrictive temperature of 25°C to select for F2 animals carrying transgenes. When unsequenced PCR products were used to generate transgenes, a mixture of at least six independent reactions was used.

The *sel-2* genomic region (extending until the next gene on either side) was PCR amplified and injected (10 ng/μl) into *sel-2*(*n655*) hermaphrodites together with *myo-3*p*::gfp* (20 ng/μl) or *ttx-3*p*::gfp* (60 ng/μl) as the only co-injection markers. Rescue of the *sel-2*(–) *lin-12*(*n302*) Muv phenotype was assessed by crossing each array into the double mutant and scoring the number of pseudovulvae in animals with or without the array.

The transcriptional reporter for *sel-2* was generated by overlapping PCR: the 5′ flanking region extending until the next gene was fused to the coding sequence of YFP containing two nuclear localization sequences (2XNLS-YFP) and injected at 50 ng/μl.

We generated the large (22 kb) translational reporter for *sel-2* using two PCR fragments covering the rescuing *sel-2* genomic region, such that they overlapped by ~1 kb. The upstream fragment included the 5′ flanking region of *sel-2* followed by approximately half the *sel-2* gene, and the downstream fragment included the other half of the *sel-2* gene with the coding sequence for GFP inserted just before the stop codon, followed by the *sel-2* 3′ flanking region. Either one or both fragments were injected at 5 ng/μl together with *ttx-3::gfp* at 60 ng/μl. Transgenic arrays generated by co-injecting both fragments rescued the Muv phenotype of *sel-2*(*n655*) *lin-12*(*n302*) (3/7 lines) and expressed GFP, presumably because of recombination in the overlapping regions of the co-injected fragments, whereas arrays including only one of the two fragments did not (0/7 lines for the N-terminal fragment, 0/6 lines for the C-terminal fragment).

lin-12(*n302*)*::gfp* was prepared by subcloning the relevant PCR-amplified region from *lin-12*(*n302*) hermaphrodites into the *lin-12::gfp* construct (Levitan and Greenwald, 1998), and was injected at 5 ng/μl. Basolaterally targeted *lin-12::gfp* and *lin-12*(*n302*)*::gfp* were generated by fusing the coding sequence for the carboxy-terminus of the LET-23 receptor – upstream primer: 5′-CCCCAACTTTTCCTGGAAAATTC, downstream primer: 5′-AAGACAAGTTTCCTTTTGTGATAC – to the 3′ end of *lin-12::gfp* (Levitan and Greenwald, 1998) or *lin-12*(*n302*)*::gfp* (this study) and injected at 5 ng/μl.

RNAi

For *sel-2*(*RNAi*), the genomic region covering exons 8-21 was amplified and cloned into the double T7 promoter plasmid pPD129.36 (Timmons et al., 2001). For *asb-1*(*RNAi*) and *apc-11*(*RNAi*), the entire genomic region of each gene was amplified and cloned into pPD129.36. As a negative control, the coding sequence of GFP was used. These constructs were transformed into HT115 bacteria and used for RNAi by feeding as described (Timmons et al., 2001) except that overnight cultures were used directly without IPTG induction in liquid culture and NGM agar plates contained fresh IPTG at 5 mmol/l. L4 larvae were placed onto lawns of the relevant bacteria and their progeny were scored.

Immunofluorescence staining and microscopy

The procedure of Bettinger et al. (Bettinger et al., 1996) was used, except that 1% formaldehyde and 0.1% Triton was used for staining of LET-23. Eggs were collected by bleaching and grown at 20°C for 41 hours before fixation of larvae. Anti-GFP (Molecular Probes) was used at 1:300; MH27 (Developmental Studies Hybridoma Bank, University of Iowa) was used at

1:1000 for the purified antibody and at 1:10 for unpurified supernatant; anti-LET 23 (Whitfield et al., 1999), kindly provided by S. Kim, was used at 1:2000. All fluorescently labeled secondary antibodies (Jackson Immunochemicals) were used at 1:300 dilution. Image acquisition was on a Zeiss Axioplan 2 microscope with a Hamamatsu ORCA100 camera, a Zeiss Z1 microscope with an ApoTome attachment and a Hamamatsu ORCA–ER, or a Biorad MRC 1024 ES confocal set-up attached to a Nikon Eclipse E800 microscope. All images subject to comparison were identically acquired and processed.

Quantification of LIN-12::GFP fluorescence intensity

A 63× 1.4 N.A. Planapochromat objective on a Zeiss Z1 microscope with ApoTome attachment was used to acquire Z-slices at a distance of 0.36-0.38 μm through VPC descendants of fixed and stained worms at the Pn.px stage. Quantification was done using Zeiss AxioVision 40 Version 4.5 software. A region of interest (ROI) designating two VPC descendants at the Pn.px stage was manually defined in the slice where the cells cover the maximum area, and the signal in all slices was summed to obtain the total LIN-12::GFP fluorescence intensity for those two cells. An ROI of identical area in a nonexpressing section of the worm was used to define the background, which was also summed in all slices and subtracted from the total LIN-12::GFP fluorescence. The normalized total fluorescence was compared between genotypes. For *sel-2*(+)*; sel-10*(+) hermaphrodites, the intensity in arbitrary units (AU) of the Pn.px cell pairs averaged 89.9±13.2 (s.e.m., n=14); for *sel-2*(–), the intensity averaged 149.1±10.4 (n=21); and for *sel-10*(–), 112.9±11.0 (n=16). The difference in intensity between *sel-2*(+) and *sel-2*(–) hermaphrodites is statistically significant (P<0.01 in an unpaired, two-tailed Student's t-test).

As there is some variability between worms in the size and shape of the Pn.px cells, the number of Z-slices varied slightly from animal to animal (13-20 slices). In all three genotypes, the cells quantified were P4.px, P5.px, P7.px or P8.px, either in a ventral or lateral view. There is no significant difference in fluorescence intensity between secondary and tertiary cells within a particular genotype. To avoid bias, images of the first five Pn.px stage worms on each slide were acquired for quantification, and the acquisition was carried out blind to genotype.

Table 1. *sel-2* loss-of-function enhances *lin-12(d)* alleles in the VPCs

Relevant genotype*	%Muv (n)†	Pseudovulvae‡
N2	0 (many)	0
sel-2(n655)	0 (many)	0
sel-2(ar219)	0 (many)	0
lin-12(n302)	2 (230)	0.37
sel-2(n655) lin-12(n302)	100 (103)	4.7
sel-2(ar219) lin-12(n302)	100 (105)	5.3
lin-12(n379)	14 (102)	0.92
sel-2(n655) lin-12(n379)	66 (103)	2.8
sel-2(ar219) lin-12(n379)	80 (112)	3.2
lin-12(n676)	21 (96)	1.3
sel-2(n655) lin-12(n676)	100 (53)	4.4
sel-2(ar219) lin-12(n676)	93 (57)	4.2
sel-2(+); arIs12§ (20°C)	0 (107)	0.18
sel-2(n655); arIs12 (20°C)	0 (107)	0.16
sel-2(ar219); arIs12 (20°C)	0 (107)	0.15
sel-2(+); arIs12 (15°C)	56 (133)	2.6
sel-2(n655); arIs12 (15°C)	61 (124)	2.7
sel-2(ar219); arIs12 (15°C)	58 (115)	2.6

*All *lin-12(n379)* and *lin-12(n676)* strains also carry *dpy-17(e164)*.
†Muv defined as ⩾3 pseudovulvae.
‡Average number of pseudovulvae.
§*arIs12[lin-12(intra)]* expresses the intracellular domain of LIN-12 under the control of *lin-12* regulatory sequences.

Endocytosis assays in the intestine

To assess endocytosis from the apical surface of the intestine, young adult hermaphrodites were incubated in a drop of TMRE-dextran (0.1 mg/ml) or FM4-64 (0.4 mmol/l) in buffer (118 mmol/l NaCl, 48 mmol/l KCl, 2 mmol/l $MgCl_2$, 2 mmol/l $CaCl_2$, 10 mmol/l HEPES, pH 7.4) for 4-5 hours, allowed to recover on NGM plates seeded with OP50 bacteria for 120 minutes in the

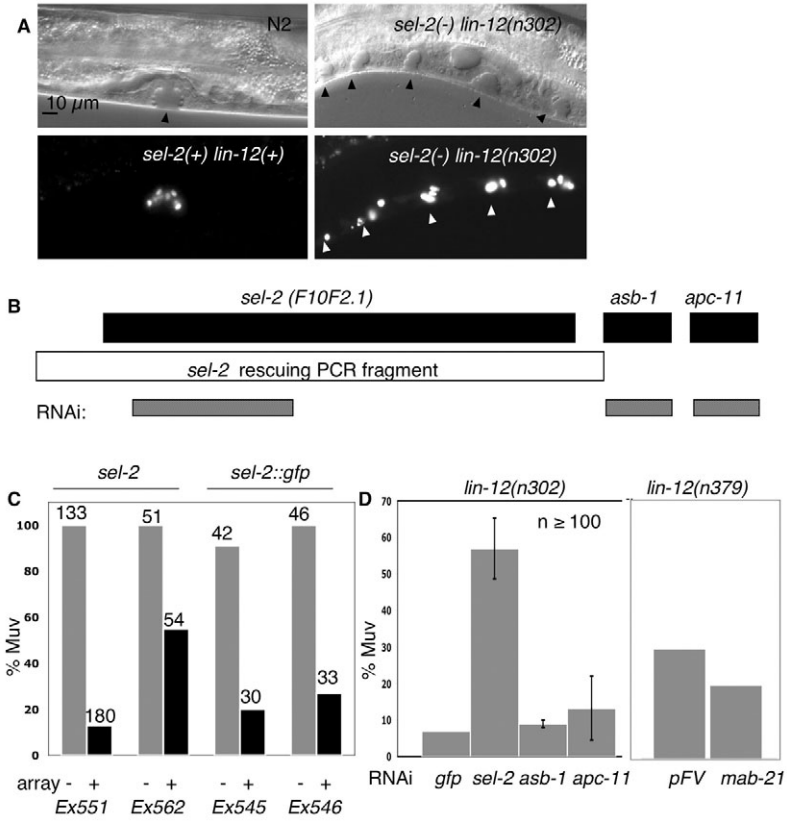

Fig. 1. *sel-2* loss of function enhances *lin-12*(*d*) activity in VPCs. (**A**) Late L4 stage N2 (left) and *sel-2*(*n655*) *lin-12*(*n302*) (right) hermaphrodites. Top panels show Nomarski photomicrographs, with the arrow(s) indicating a normal vulva (N2) or pseudovulval invaginations; bottom panels show clusters of cells expressing *egl-17::cfp-lacZ* (*arIs92*). (**B**) Schematic view of the predicted *sel-2* operon, indicating the regions used for rescue and RNAi experiments. (**C**) The *sel-2* genomic region and a *sel-2* translational reporter 'rescue' the enhancement of *lin-12*(*n302*) by *sel-2*(*n655*). Arrays are described in Materials and methods. Multivulva (Muv) is defined as ⩾3 pseudovulvae. The number of worms scored is indicated above each bar. (**D**) *sel-2*(*RNAi*) enhances *lin-12*(*d*). pFV denotes the empty RNAi feeding vector. Except for *mab-21*(*RNAi*), each bar represents the mean of at least two independent experiments; error bars are the s.e.m. Muv is defined as ⩾2 pseudovulvae; a minimum of 100 animals was scored for each treatment.

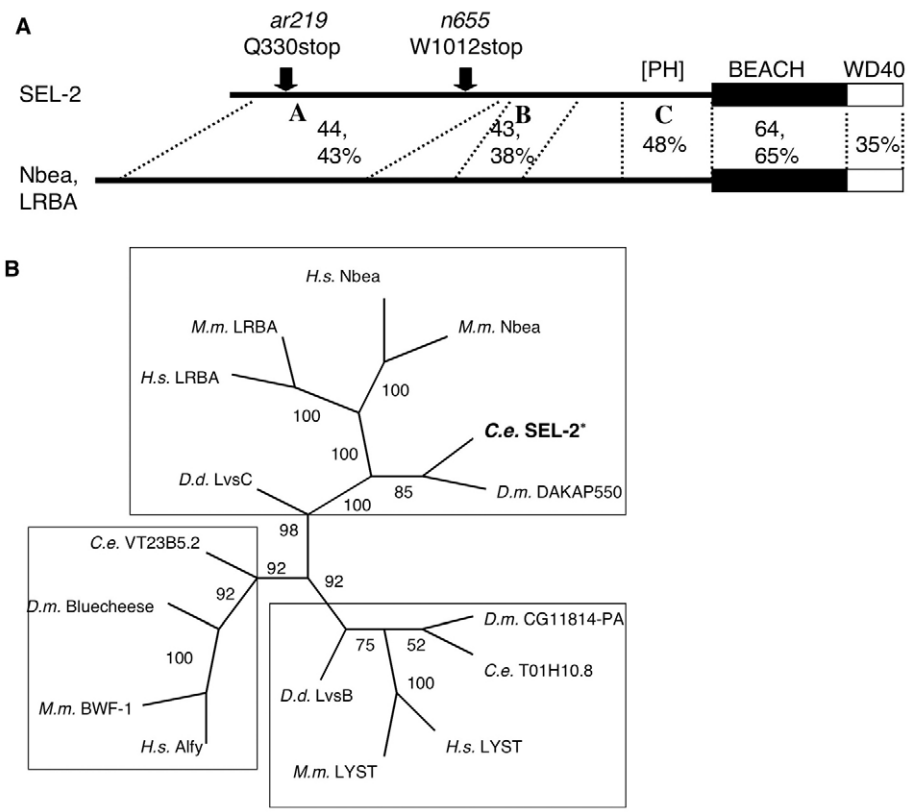

Fig. 2. *sel-2* sequence analysis.
(**A**) Comparison of SEL-2 with mammalian neurobeachin and LRBA. The % amino acid identity is indicated for the BEACH and WD40 domains, and for other regions of high homology designated 'A', 'B' and 'C' (aa 164-1036, 1059-1306, and 1407-1828 in SEL-2, respectively). Region C includes the predicted PH domain of neurobeachin and LRBA (see text). We note that neurobeachin and DAKAP550 have been shown to bind to the regulatory domain (RII) of PKA with high affinity in vitro (Han et al., 1997; Wang et al., 2000b), whereas LRBA does not (Wang et al., 2000b). The RII-binding region of neurobeachin lies in the unconserved interval between homology regions A and B. (**B**) Phylogenetic bootstrap tree constructed from an alignment of the C-terminal regions (see Materials and methods) of *C. elegans* (*C.e.*) SEL-2, VTB23.5 and T01H10.8 and their homologs. Numbers at the nodes are bootstrap values, indicating the frequency of occurrence of a given partition in the 100 replicate trees. Boxed areas represent subfamilies of BEACH domain-containing proteins. Species are designated as follows: *D.m.*, *Drosophila melanogaster*; *H.s.*, *Homo sapiens*; *M.m.*, *Mus musculus*; *D.d.*, *Dictyostelium discoideum*.

dark, then mounted in M9 supplemented with 10 mmol/l levamisole and imaged. To assess endocytosis from the basolateral surface of the intestine, the dyes were prepared as above, injected into the pseudocoelom of ≅10 L4 hermaphrodites at a time and the animals were mounted and imaged 10 minutes after injection (Fares and Grant, 2002; Hermann et al., 2005).

RESULTS

sel-2 is a negative regulator of *lin-12* activity in the VPCs

Semidominant missense *lin-12* mutations that cause constitutive activity form an allelic series (Greenwald and Seydoux, 1990; Greenwald et al., 1983). The phenotype caused by these mutations in *C. elegans* hermaphrodites largely reflects the degree of constitutive activity of the receptor. When LIN-12 constitutive activity is low, the gonadal anchor cell is not specified and all of the VPCs take on the non-vulval 3° fate, resulting in a 'Vulvaless' (Vul) phenotype. However, when LIN-12 constitutive activity is high, all VPCs become 2°, even though there is no anchor cell. The descendants of each 2° VPC undergo morphogenesis to form a pseudovulva, resulting in a 'Multivulva' (Muv) phenotype.

sel-2(*n655*) was isolated after EMS mutagenesis of *lin-12*(*n302*), an allele that normally causes a Vul phenotype. Although in the somatic gonad there may be slight suppression (<1%) of the lack of an AC caused by *lin-12*(*n302*) (data not shown), the striking feature of the *sel-2*(*n655*) *lin-12*(*n302*) double mutant is that it displayed a completely penetrant Muv phenotype (Table 1; Fig. 1A). This result suggests that *sel-2*(*n655*) enhances *lin-12*(*n302*) activity in the VPCs.

The apparent enhancement of *lin-12* activity in the VPCs is neither *sel-2* nor *lin-12* allele-specific. *sel-2*(*ar219*), identified in a non-complementation screen (see Materials and methods), also enhanced *lin-12*(*n302*) (Table 1). Furthermore, when either *sel-2* allele was combined with other *lin-12* alleles that cause a Vul phenotype, the resulting double mutant was Muv (Table 1). In these double mutants, the morphology of the pseudovulvae and expression of a 2° fate marker indicated that each VPC had adopted a 2° fate (Fig. 1A). As described below, the molecular characterization of *sel-2*(*n655*) and *sel-2*(*ar219*) indicated that they are null alleles. Thus, loss of *sel-2* activity enhanced *lin-12* activity, suggesting that *sel-2* is a negative regulator of *lin-12* activity in the VPCs.

Genetic evidence suggests that *sel-2* is not involved in the same processes that are affected by the other negative regulators of *lin-12* studied so far: proteasomal degradation (*sel-10*), endoplasmic reticulum (ER) associated degradation (*sel-1*) and quality control at the ER (*sel-9*). *sel-2*(–), unlike *sel-10*(–) (Hubbard et al., 1997), did not enhance the activity of *lin-12*(*intra*), a constitutively active cytosolic form of LIN-12 (Table 1) (N.d.S., H.F. and I.G., unpublished). *sel-2*(–), unlike *sel-1*(–) (Urano et al., 2002), did not cause upregulation of ER chaperones at the transcriptional level (data not shown). Finally, *sel-2*(–), unlike *sel-9*(–) (Wen and Greenwald, 1999), did not suppress the phenotype of *glp-1*(*q415*), in which the LIN-12 paralog GLP-1 accumulates intracellularly in the gonad at the restrictive temperature (data not shown). Instead, as described herein, *sel-2* may function as a negative regulator of *lin-12* activity through an effect on endocytic traffic.

Molecular identification of *sel-2*

sel-2 was mapped to a region encompassing four predicted ORFs (see Materials and methods). Sequencing of these genes in *sel-2*(*n655*) identified a nonsense mutation (W1012stop) in exon 12 of *F10F2.1*, and *sel-2*(*ar219*) has a nonsense mutation (Q330stop) in exon 8 (Fig. 2A). F10F2.1 is the first gene in a predicted operon, which includes *asb-1*, a homolog of ATP synthase B, and *apc-11*, a subunit of the anaphase promoting complex (Fig. 1B). *mab-21* (Chow et al., 1995) is a small gene located in the opposite orientation in the 22nd intron of F10F2.1. Three lines of evidence indicate that F10F2.1 is *sel-2*. First, both *sel-2* alleles contain stop codons in this

predicted gene (see also below). Second, extrachromosomal arrays carrying the genomic region of F10F2.1 rescued the Muv phenotype of *sel-2*(–) *lin-12*(*n302*) (Fig. 1C). Third, reduction of *sel-2* activity, but not of *asb-1*, *apc-11* or *mab-21* activity, by RNAi resulted in a Muv phenotype in *lin-12*(*n302*) or *lin-12*(*n379*) animals (Fig. 1D).

F10F2.1 has two striking amino acid motifs, a Beige and Chediak-Higashi (BEACH) domain, and four repeated WD40 motifs. The crystal structure of the BEACH domain from both human neurobeachin and LRBA indicates that this domain has an unusual polypeptide backbone fold, and is immediately preceded by a novel Pleckstrin Homology (PH) domain that is not recognizable by primary amino acid sequence analysis (Jogl et al., 2002; Gebauer et al., 2004). A WD40 motif folds into a 'β-propeller blade', and tandem copies form a multibladed propeller structure that is thought to mediate protein-protein interactions (Sondek et al., 1996; Wall et al., 1995). The BEACH-WD40 region is positioned at the carboxy terminus of the protein. Both *sel-2* mutants are predicted to encode truncated proteins that would lack the BEACH-WD40 region (Fig. 2A).

Reciprocal BLAST searches and sequence alignments using either the entire protein or only the carboxy terminal BEACH-WD40 domain indicated that SEL-2 has homologs in several eukaryotes, including *Drosophila* DAKAP550 and mammalian neurobeachin and LRBA. There are several regions of high conservation between SEL-2 and its mammalian homologs throughout the length of the protein (Fig. 2A), with 64-65% amino acid identity in the BEACH domain, as well as 48% identity in 'homology region C', which includes the PH domain that was structurally defined for neurobeachin and LRBA. We could not conclude whether SEL-2 is more 'neurobeachin-like' or 'LRBA-like' based on sequence analysis (Fig. 2A,B).

SEL-2/neurobeachin/LRBA appears to form a subfamily within a larger family of BEACH-WD40 domain-containing proteins. There are three other *C. elegans* BEACH-containing proteins (Fig. 2B and data not shown). The most closely related to SEL-2 is VT23B5.2, the ortholog of human ALFY (WDFY3 – Human Gene Nomenclature Committee) (Simonsen et al., 2004) and *Drosophila* Blue Cheese (Finley et al., 2003), consisting of little else but the BEACH domain and five WD40 motifs, plus a C-terminal FYVE domain. The *VT23B5.2*(*ok912*) null allele (kindly provided by the Knockout Consortium) did not have a readily discernable visible phenotype on its own or in a double mutant with *sel-2*(–), and did not cause a Muv phenotype in combination with *lin-12*(*n379*), suggesting that SEL-2 and VT23B5.2 are not functionally redundant (data not shown). The two other BEACH-containing proteins in *C. elegans* are T01H10.8, the apparent ortholog of mammalian LYST (Nagle et al., 1996), although it (unlike LYST) does not have predicted WD40 motifs, and F52C9.1, which has only two WD40 motifs.

SEL-2 expression and subcellular distribution

A transcriptional reporter for *sel-2* in which the 5′ upstream region drives nuclearly localized YFP is expressed in the VPCs and their descendants (Fig. 3A,B), as well as in many other cell types, including the epithelial cells of the intestine (Fig. 3C,D) and the rectum, the seam cells, many cells in the head and the tail, and the cells of the ventral nerve cord (not shown). In live worms, expression of a rescuing SEL-2::GFP translational reporter (Fig. 1C; also see Materials and methods) was strongest in the rectal epithelial cells (Fig. 3E,F) and in the seam cells (not shown), where it appeared to be distributed throughout the cytoplasm, but particularly concentrated close to the nucleus. This distribution is consistent with partial membrane association of SEL-2::GFP, as has previously been proposed for its mammalian homologs neurobeachin and LRBA (Wang et al., 2001; Wang et al., 2000b).

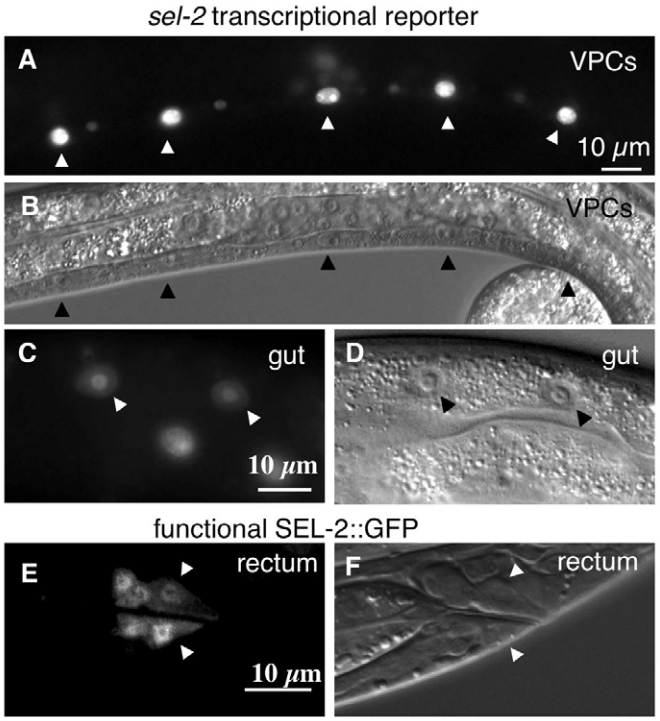

Fig. 3. *sel*-2 expression. The 5′ flanking region of *sel-2* drives expression of NLS-YFP in several cell types, including VPCs in an L2 or L3 larva (**A**,**B**) and intestinal epithelial cells in an L4 larva (**C**,**D**). SEL-2::GFP expression is shown in the rectal epithelia in a live L2 or L3 larva (**E**,**F**).

sel-2 affects the subcellular localization of LIN-12::GFP in VPCs

We examined the subcellular localization of LIN-12::GFP in the VPCs and their descendants in *sel-2*(+) and *sel-2*(–) hermaphrodites (Fig. 4), using the adherens junction protein AJM-1 and LET-23/EGFR for comparison. The adherens junctions are circumferential, close to the apical surface of the VPCs. LET-23 is localized basolaterally at the Pn.px stage, except in P6.px, where it is also present at the apical surface (Whitfield et al., 1999). It is expressed strongly in P6.px and weakly in the other VPC descendants at this stage.

In *sel-2*(+), LIN-12::GFP was mostly at the apical surface of the VPCs or in puncta close to the apical surface (Fig. 4C,D, top panel; 36% of animals had visible non-apical LIN-12::GFP, *n*=292), and did not co-localize appreciably with the basolateral LET-23/EGFR (Fig. 4E,F, top panel). By contrast, in *sel-2*(–), LIN-12::GFP was not restricted to the apical surface but was also present basolaterally (Fig. 4C,D, bottom panel, see arrows; 89% of animals had visible non-apical LIN-12::GFP; *n*=154) and indeed appeared to co-localize with LET-23 at the basolateral membrane (Fig. 4E,F, bottom panel, see arrows). The VPCs seemed to be polarized normally in *sel-2*(–), as LET-23/EGFR displayed its typical distribution (Fig. 4E,F; red channel), and the adherens junctions appeared normal (Fig. 4C,D; red channel).

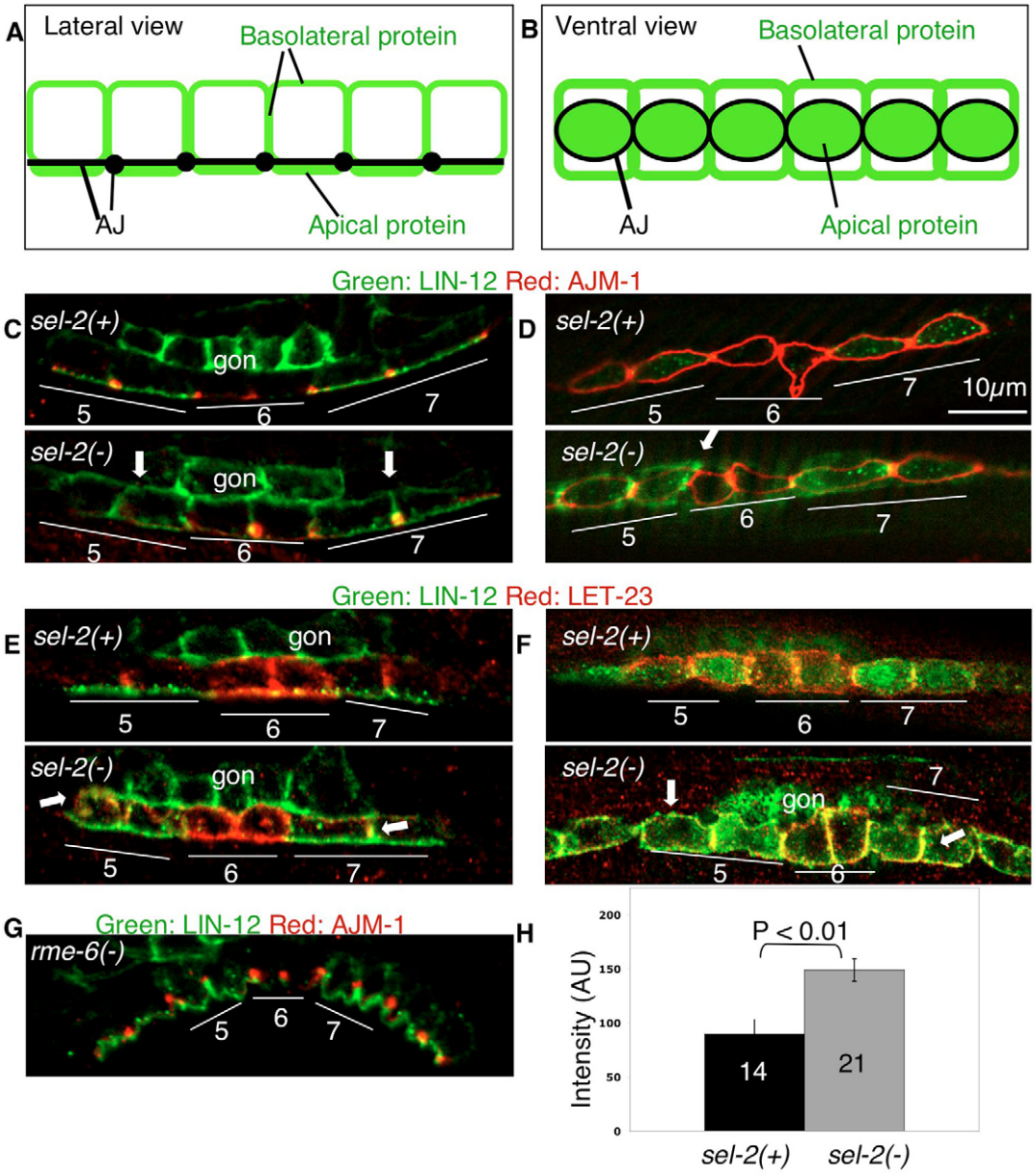

Fig. 4. LIN-12::GFP and LET-23 localization. (**A**,**B**) Schematic depiction of the localization of an apical or a basolateral protein in the VPCs relative to the adherens junction (AJ) in a lateral (A) or a ventral view (B). (**C**) Lateral and (**D**) ventral views of the distribution of LIN-12::GFP expressed from *arls41* (green) relative to the AJ (red). (**E**) Lateral and (**F**) ventral views of LIN-12::GFP (green) and LET-23 (red). (**G**) Lateral view of LIN-12::GFP distribution (green) in *rme-6*(*b1018*) relative to the AJ (red). (**H**) Quantification of LIN-12::GFP fluorescence intensity in *sel-2*(+) and *sel-2*(–) hermaphrodites (see Materials and methods). In photomicrographs, 'gon' marks LIN-12::GFP staining in the gonad, which is close to the basolateral surface of the VPCs, and arrows indicate basolateral LIN-12::GFP. P5.px, P6.px and P7.px are indicated.

In addition to being mislocalized to the basolateral surface, the overall level of LIN-12::GFP was elevated in *sel-2*(–) in fixed and stained (Fig. 4) or live, unstained animals (not shown). Indeed, LIN-12::GFP was often undetectable in the VPCs of unstained *sel-2*(+) animals in VPCs and their descendants but could be detected at both apical and basolateral surfaces of the VPCs in live *sel-2*(–) animals. Quantification of LIN-12::GFP fluorescence intensity showed significantly higher levels in VPC descendants of *sel-2*(–) versus *sel-2*(+) animals at the Pn.px stage (Fig. 4H; see Materials and methods).

LIN-12::GFP accumulation at the basolateral surface of the VPCs is not sufficient to increase *lin-12* activity

To test whether basolateral mislocalization of LIN-12 in the VPCs is sufficient to increase *lin-12* activity, we added the basolateral targeting sequence (BL) of LET-23 (Kaech et al., 1998) to LIN-12::GFP. LIN-12::GFP-BL accumulated basolaterally (Fig. 5A) and was able to rescue *lin-12*(*0*) defects (not shown), indicating that the added amino acids do not eliminate *lin-12* activity. Hermaphrodites expressing LIN-12::GFP-BL were not Muv (Fig. 5B), suggesting that basolateral localization is not sufficient to activate the receptor.

We also tested whether basolateral targeting of a constitutively active form of LIN-12 makes it refractory to loss of *sel-2* activity, as might be the case if *sel-2*(–) enhances *lin-12*(*n302*) activity simply by misrouting it to the basolateral domain. Hermaphrodites expressing LIN-12(n302)::GFP or LIN-12(n302)::GFP-BL were Muv to the same extent, consistent with the results described above suggesting that basolateral targeting per se does not activate LIN-12 (Fig. 5B). Moreover, the Muv phenotype of LIN-12(n302)::GFP-BL animals was further enhanced in a *sel-2*(*n655*) background (Fig. 5C). As LIN-12(n302)::GFP-BL was significantly basolateral in all VPCs in the majority of *sel-2*(+) animals examined, the results suggest that the effect of *sel-2* on *lin-12* activity is not solely due to the basolateral accumulation of LIN-12 in *sel-2*(–), subject to the caveat that an effect on untagged LIN-12(+) protein may be contributing to this enhancement.

sel-2 and regulated endocytic traffic in the VPCs

We examined the consequences of loss of *sel-2* on the two regulated endocytic events in VPCs described in the Introduction. When LET-23/EGFR is activated in P6.p by the inductive signal, LIN-12 internalization and downregulation via the multivesicular endosome sorting pathway is stimulated (Shaye and Greenwald, 2005). LIN-12::GFP was downregulated to the same extent in *sel-2*(+) and *sel-2*(–) hermaphrodites (Fig. 6A), suggesting that *sel-2* is not required for LET-23-dependent internalization or downregulation of LIN-12 from the apical surface. However, *sel-2* activity appears to be required for efficient downregulation of basolateral LIN-12::GFP-BL, as a greater proportion of *sel-2*(–)hermaphrodites retain substantial fluorescence in P6.px (Fig. 6A).

We also examined downregulation of endogenous LET-23 in the VPC descendants. When LIN-12 is activated in P5.p and P7.p by the lateral signal, LET-23/EGFR is downregulated (Stetak et al., 2006; Whitfield et al., 1999). By contrast, in a *sel-2*(–) mutant, LET-23/EGFR appears to accumulate aberrantly in P5.p and P7.p (Fig. 6C). At both the Pn.px and the Pn.pxx stage, a smaller fraction of *sel-2*(*ar219*) worms (44%, *n*=52 at Pn,px) as compared to wild type (74%, *n*=79 at Pn.px) had no detectable LET-23 in the descendants of P5.p and/or P7.p (Fig. 6B). A similar effect was seen in *sel-2*(*n655*) (data not shown). However, we did not detect any evidence of ectopic LET-23/EGFR activity in P5.p or P7.p, as assayed by ectopic expression of a LET-23 target gene (data not shown).

In addition to these regulated events that occur in response to intercellular signals, LIN-12 appears to be constitutively internalized, and recycled or degraded at a basal level in all VPCs (Shaye and Greenwald, 2005). To examine the effect of reducing constitutive endocytosis, we removed the activity of *rme-6*, a regulator of Rab5 found in coated pits (Sato et al., 2005). We found that *lin-12* activity was enhanced by loss of *rme-6*: 21% of *lin-12*(*n302*)*; rme-6*(*b1018*) were Muv (*n*=106), compared with 2% of *lin-12*(*n302*) animals (*n*=104). However, LIN-12::GFP did not accumulate at the basolateral surface of the VPCs (Fig. 4G), suggesting that *rme*-6, which functions in traffic from the plasma membrane to early endosomes, behaves differently from *sel-2*.

sel-2 and endocytic traffic in the intestine

sel-2 is expressed in cells of the intestine, which like the VPCs, are polarized epithelial cells. Endocytic traffic from either the apical or the basolateral surfaces of the intestinal epithelium may be observed after the delivery of marker dyes by feeding (apical) or injection into the pseudocoelom (basolateral) (Fares and Grant, 2002). A prominent feature of intestinal cells is the presence of autofluorescent 'gut granules', which have been shown to be lysosomes (Clokey and Jacobson, 1986; Grant et al., 2001). The membrane-intercalating dye FM4-64 accumulates in these structures when delivered apically or basolaterally (Grant et al., 2001; Fares and Grant, 2002; Hermann et al., 2005). Fluid-phase markers accumulate in these structures when delivered apically, but not basolaterally due to rapid recycling to the pseudocoelom (Fares and Grant, 2002).

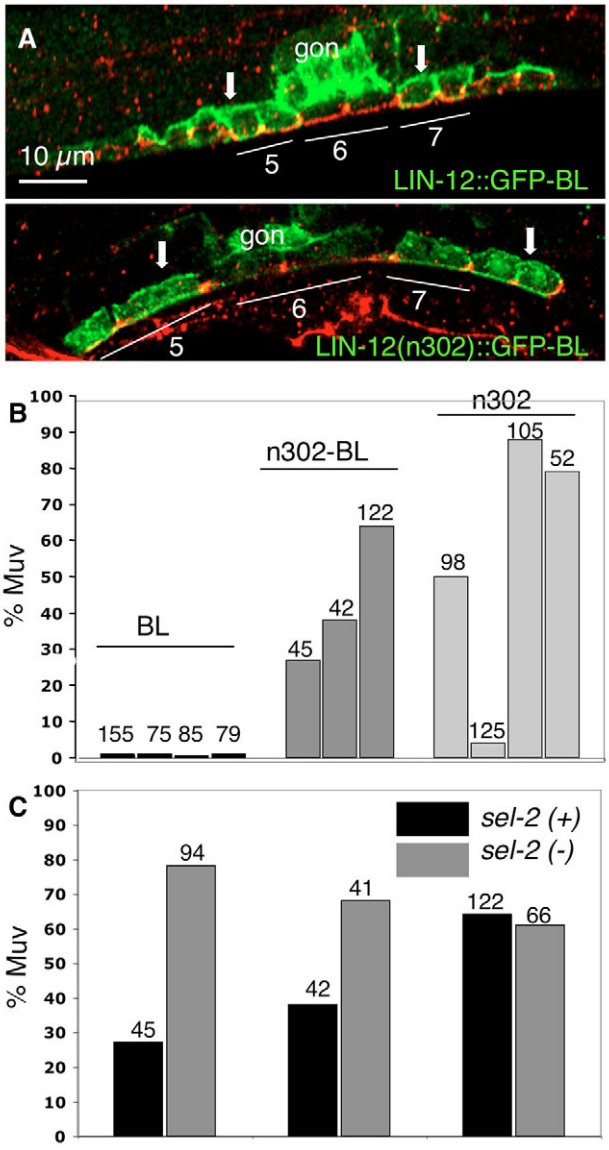

Fig. 5. LIN-12::GFP targeted to the basolateral surface of the VPCs. (**A**) Lateral views of Pn.px hermaphrodites showing LIN-12::GFP-BL (upper panel) and LIN-12(n302)::GFP-BL (lower panel) in green, and the adherens junctions (AJM-1) in red. 'gon' marks LIN-12::GFP staining in the gonad. The basolateral surface of some cells is indicated with arrows. P5.px, P6.px and P7.px are indicated. (**B**) Each bar represents an independent transgenic line expressing the indicated protein. (**C**) The percentage of Muv animals in three independent transgenic lines carrying LIN-12(n302)::GFP-BL in *sel-2*(+) and *sel-2*(*n655*) backgrounds is plotted. The number above each bar is the number of animals scored. Muv is defined as ⩾3 pseudovulvae.

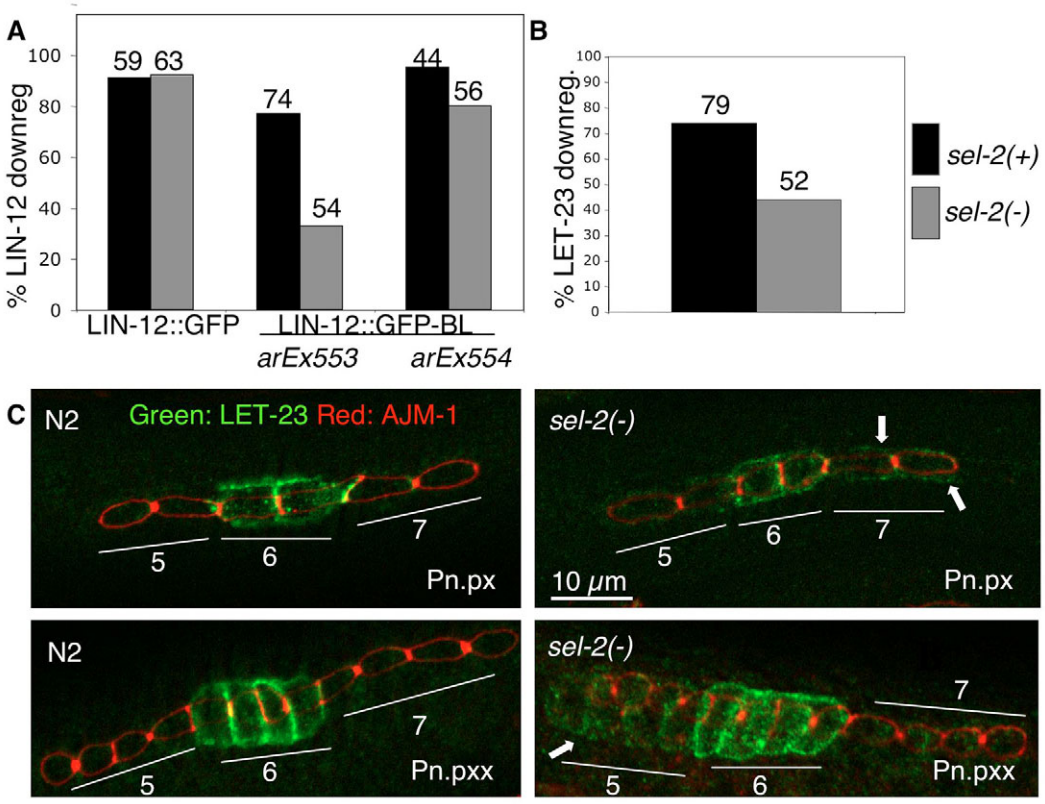

Fig. 6. Regulated endocytosis in *sel-2*(*ar219*). (**A**) The fraction of animals with LIN-12::GFP or LIN-12::GFP-BL downregulated in P6.px is plotted. (**B**) The fraction of animals with LET-23 downregulated in P5.px and P7.px is plotted. For both graphs, numbers above the bars are the number of animals scored. In (**C**), endogenous LET-23 is shown in green and the adherens junction (AJM-1) is in red. Arrows indicate persistent LET-23 expression. P5.p, P6.p and P7.p descendants are indicated.

FM4-64 delivered to the pseudocoelom concentrated in a different pattern in the intestine of *sel-2*(*n655*) and *sel-2*(*ar219*) compared with wild type (Fig. 7), suggesting an alteration in endocytic traffic from the basolateral surface. In wild-type animals imaged 10-30 minutes after injection, FM4-64 concentrated in defined punctate structures, which partially overlap with autofluorescent gut granules. By contrast, FM4-64 compartments in *sel-2*(–) were irregularly shaped, largely not overlapping with autofluorescent granules, and predominantly clustered at the apical surface of the intestinal epithelium (Fig. 7A,B). These experiments were performed on mixed populations of *sel-2*(+) and *sel-2*(–) hermaphrodites, blind to genotype. *sel-2*(+) worms were identified after scoring by the presence of *ttx-3*::GFP expressed in a single neuron in the head of the worm: 85% of *sel-2*(*ar219*) (n=33) and 89% of *sel-2*(*n655*) (n=9) had the '*sel-2* phenotype' compared with 0% of *sel-2*(+) (n=42) (Fig. 7C). Furthermore, the phenotype was partially rescued by an extrachromosomal array expressing the *sel-2* genomic region (1 out of 2 lines) and also partially reproduced in wild-type animals by *sel-2*(*RNAi*) (43%, n=23) but not by control *GFP*(*RNAi*) (0%, n=25) conducted in parallel (Fig. 7C). These observations suggest that there is a perturbation in endosomal traffic or in endosomal membrane organization in the intestinal epithelium of *sel-2* (–) animals.

FM4-64 accumulation was more similar to wild type when *sel-2*(–) animals were imaged 2-2.5 hours after injection of the dye (46% of animals are mutant for FM4-64 distribution at t120 minutes, n=26, compared with 85% at t0, n=13), suggesting that the FM4-64 compartment in *sel-2*(–) may be pre-lysosomal and that *sel-2* affects the rate of some step in endosomal traffic. Injection into the pseudocoelom of fluorescent dextran, a fluid-phase marker, did not reveal any defects in *sel-2*(–) hermaphrodites (data not shown), suggesting that endocytic recycling is not the main affected step (Grant et al., 2001; Fares and Grant, 2002).

There was no obvious difference in the distribution of FM4-64 when delivered to the apical surface of the intestinal epithelium of *sel-2*(–) hermaphrodites by feeding (not shown). However, it is possible that the timescale of these experiments (feeding of dye for 4 hours, followed by a 'chase' of 2 hours to clear excess dye from the gut lumen) makes it difficult to see a small difference in rates of traffic between wild-type and *sel-2* animals. Feeding the fluid-phase marker also did not reveal any difference between wild-type and *sel-2*(–) hermaphrodites, with the same potential caveat about timescale.

The intestines of *sel-2*(–) worms appeared visually normal, and the distribution of markers for the early (RAB-5) (Zerial and McBride, 2001), late (RAB-7) (Chen et al., 2006) and recycling (RAB11, RME-1) (Casanova et al., 1999; Grant et al., 2001; Chen et al., 2006) endosomal compartments appeared qualitatively normal (not shown). Further, there is no significant perturbation in acidic organelles, as assessed by Lysotracker staining, in *sel-2*(–) (data not shown). These observations at steady-state are consistent with the loss of *sel-2*, resulting in a modest effect on traffic rates.

DISCUSSION

We have shown that *sel-2* acts as a negative regulator of *lin-12/Notch* activity in the VPCs, and that SEL-2 is the homolog of two closely related mammalian proteins, neurobeachin (also known as BCL8B) and LRBA. SEL-2, neurobeachin and LRBA form a subfamily

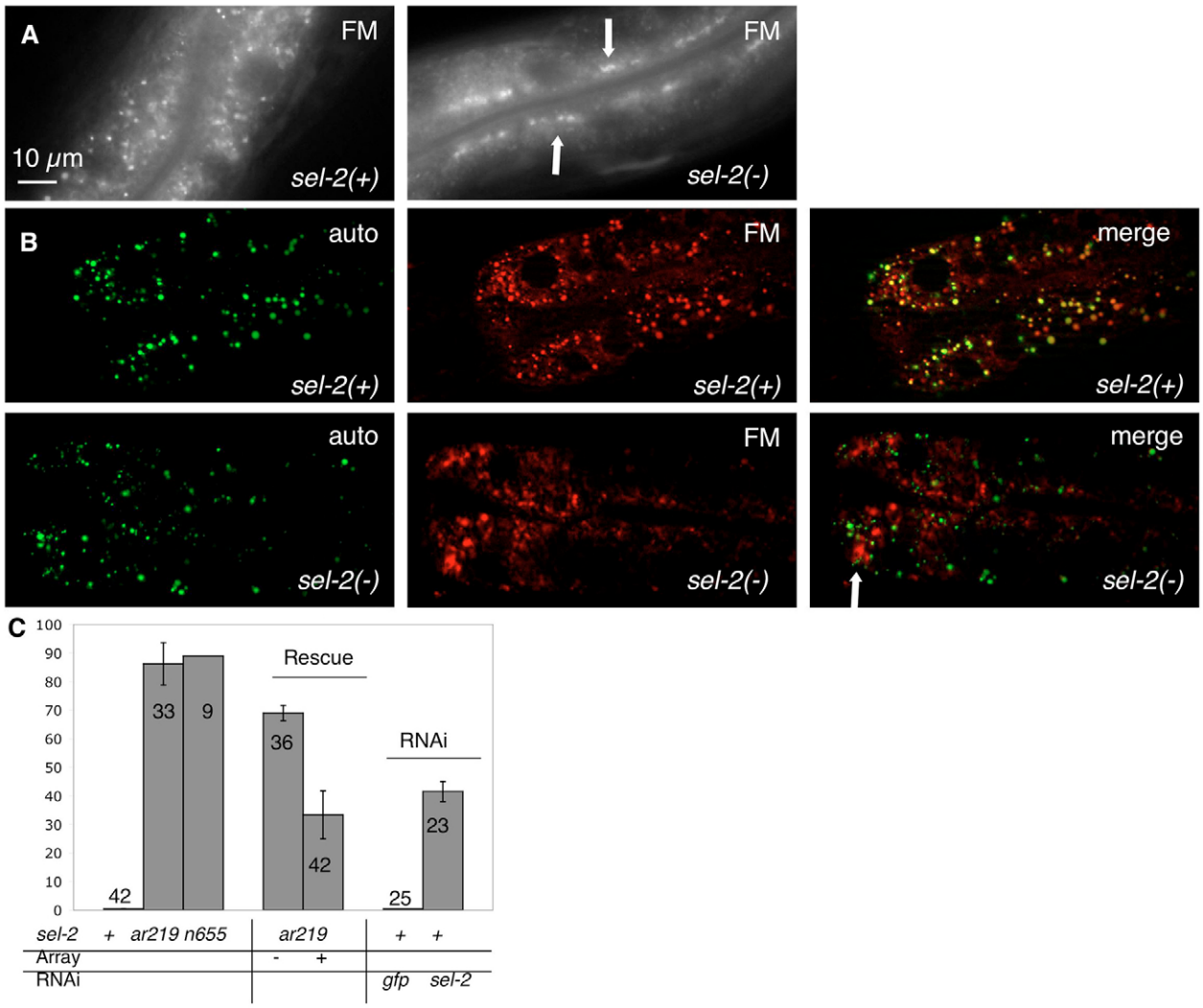

Fig. 7. Accumulation of FM4-64 in the intestine after injection into the pseudocoelom (basolateral delivery). (**A**) FM4-64 fluorescence in *sel-2*(+) and *sel-2*(*ar219*). (**B**) FM4-64 fluorescence (middle panel, red) is shown relative to autofluorescent granules (left panel, green); co-localized signals are shown in yellow in the merge (right panel). Arrows indicate irregularly shaped, FM4-64 labelled compartments that are not coincident with autofluorescence in *sel-2*(*ar219*). (**C**) Quantification of the *'sel-2'* mutant phenotype (see text). Rescue of the phenotype with an extrachromosomal array carrying the *sel-2* genomic region and phenocopy with *sel-2*(*RNAi*) is also shown. All scoring was done blind to genotype. Each bar is the mean of at least two independent experiments, and error bars are the s.e.m. The total number of worms scored is indicated on each bar.

within a larger family of eukaryotic proteins, characterized by a BEACH domain followed by repeated WD40 domains at the carboxy terminus. This subfamily is found in multicellular organisms but not in budding or fission yeasts. *Caenorhabditis elegans* therefore has particular value as a simple, genetically tractable system in which to study potential roles of this protein in vivo. Our analysis has provided in vivo evidence that SEL-2/neurobeachin/LRBA functions in endosomal traffic in polarized epithelial cells in *C. elegans*, and by extension, in polarized epithelial cells in other animals. Furthermore, our results suggest that *sel-2* activity contributes to the appropriate steady-state level of LIN-12 or to trafficking events that impact on receptor activation.

SEL-2/neurobeachin/LRBA and endocytic traffic in polarized epithelial cells

Several observations suggest that loss of *sel-2* activity compromises traffic in polarized epithelial cells. First, LIN-12::GFP, which is normally restricted to the apical surface, ectopically accumulated at the basolateral surface of the VPCs in *sel-2*(–) mutants. Furthermore, although endocytic downregulation of LIN-12::GFP from the apical surface in response to Ras activation in P6.p appeared to occur normally in *sel-2*(–) mutants, LIN-12::GFP-BL, which was mistargeted basolaterally by the addition of a basolateral targeting signal, was downregulated less efficiently in *sel-2*(–) mutants. Second, LET-23/EGFR, a basolateral protein that underwent endocytic downregulation in P5.p and P7.p in response to LIN-12 activation, was downregulated less efficiently in *sel-2*(–) mutants. Third, loss of *sel-2* resulted in slowed delivery of basolaterally delivered fluorescent lipid to acidic compartments in the polarized cells of the intestinal epithelium.

Many of these defects appear to point to a role for SEL-2 in endocytosis from the basolateral surface of polarized epithelial cells. At this time, we have no evidence that loss of *sel-2* activity also compromises endocytic traffic from the apical surface of polarized epithelial cells. As mentioned above, endocytic downregulation of LIN-12::GFP from the apical surface of P6.p occurred normally in

sel-2(–) mutants. Furthermore, apically delivered fluorescent lipids appeared to be distributed normally, although the long incubation time required for this assay may obscure a small effect on rates.

One model that can account for many of our observations is that in *sel-2*(–) mutants there is a primary defect in the rate of internalization from the basolateral surface of polarized epithelial cells. As LIN-12 is not generally seen in the basolateral domain in wild-type hermaphrodites but is seen in the basolateral domain in *sel-2* mutants, this model requires the assumption that at least some LIN-12 normally transits through the basolateral domain, and therefore can be seen in *sel-2* mutants because internalization is slowed. However, removing the activity of *rme-6*, a regulator of RAB-5 that mediates traffic from the plasma membrane to early endosomes, did not result in a similar accumulation of LIN-12 at the basolateral surface of the VPCs. As *rme-6* is associated with clathrin-coated vesicles (Sato et al., 2005) and is likely to be involved in both apical and basolateral endocytosis, this result suggests that a simple reduction in internalization does not lead to basolateral accumulation of LIN-12.

An alternative model that may better account for all of our observations is that aberrant basolateral protein accumulation in *sel-2*(–) results from problems in endosomal sorting. Surface proteins from the apical and basolateral domains of polarized mammalian cells are initially taken up into separate early endosomes but enter a common endosome before recycling back to their respective plasma membrane domains (Brown et al., 2000; Wang et al., 2000a). Basolateral proteins are transported directly from the common endosome back to the basolateral membrane, while apical proteins first enter the apical recycling endosome and are then delivered to the apical plasma membrane (Mostov et al., 2003; Hoekstra et al., 2004). Moreover, some fraction of surface proteins traffic to late endosomes and lysosomes for degradation, at steady state (Stahl and Barbieri, 2002). Increased traffic between the common endosome and the basolateral surface in *sel-2* mutants could result in the net accumulation of LIN-12 and LET-23 there. However, as we have also observed a reduced rate of lipid delivery to lysosomes in the intestinal epithelium of *sel-2* mutants, we favor the view that in the absence of *sel-2* activity there is a defect in traffic to late endosomes and lysosomes, rather than in recycling per se. For example, SEL-2 may function in sorting endosomes for the specification of membrane domains that will mature into late endosomes. A defect in this process would result in the slowed delivery of endocytosed membrane lipid to late endosomes and lysosomes. Furthermore, in the absence of SEL-2, transmembrane proteins such as LIN-12 and LET-23 may then segregate into tubular domains of sorting endosomes (Bonifacino and Rojas, 2006) that are destined for recycling back to the plasma membrane. Additional support for this view comes from the observation that certain mutant forms of LIN-12 that can be internalized from the apical surface but not degraded also accumulate at the basolateral surface of the VPCs (Shaye and Greenwald, 2005).

We note that acidic compartments in the intestine of *sel-2*(–) are qualitatively indistinguishable from those in wild type, consistent with a defect in traffic in the endosomal system rather than defective lysosomes themselves. Further, neither inhibition of sorting into internal vesicles of multivesicular (i.e. late) endosomes with *alx-1*(*RNAi*), nor mutation of LIN-12 lysine residues that are putative ubiquitination sites, cause basolateral localization of LIN-12::GFP (Shaye and Greenwald, 2005), suggesting that *sel-2* acts at a different step in this process. Taken together, our results suggest defective or slowed traffic in the endosomal system in *sel-2*(–). The resultant increased accumulation of LIN-12 could account for the enhancement of LIN-12 signaling revealed by the genetic interactions between *sel-2*(–) and *lin-12* mutations.

SEL-2 and regulation of *lin-12* activity

The genetic interactions between *sel-2* and *lin-12* suggest that *sel-2* behaves as a negative regulator of *lin-12* activity. In particular, loss of *sel-2* activity dramatically enhances the effect of certain *lin-12* alleles that cause constitutive activity. Loss of *sel-2* only enhances constitutive activity resulting from point mutations in the extracellular domain, i.e. forms of LIN-12 that still need to undergo proteolytic cleavage events to signal, and not the constitutive activity resulting from a truncation that mimics the end product of the cleavage events. These genetic results are consistent with a role for *sel-2* in LIN-12 trafficking either before ligand activation or in the cleavage events that occur upon ligand binding.

The observation that *sel-2* mutants are phenotypically wild type raises the question of the normal contribution of *sel-2* in regulating *lin-12* activity in VPCs. We did not see any evidence that VT23B5.2, the closest BEACH-WD40 paralog encoded in the *C. elegans* genome, is functionally redundant with SEL-2 (N. de S. and I.G., unpublished). However, it is possible that another protein is functionally redundant, or that there is an independent but redundant regulatory mechanism. Alternatively, *sel-2* may be involved in fine-tuning the level of *lin-12* activity by contributing to proper LIN-12 trafficking. In both well-studied paradigms of LIN-12 signaling in *C. elegans*, the AC/VU decision in the developing gonad or VPC fate specification in the developing vulva, the control of relative levels of the receptor in different cells is a key component of fate specification. In the AC/VU decision, regulation of LIN-12 levels occurs principally by modulating *lin-12* transcription (Wilkinson et al., 1994; Greenwald, 2005). In the VPCs, LIN-12 traffic and stability, rather than *lin-12* transcription, is modulated. It may be that in the VPCs, post-transcriptional mechanisms are better able to coordinate LIN-12 activity in lateral signaling with LET-23/EGFR activity in inductive signaling. Perhaps *sel-2* activity contributes to the delicate balance and mutual feedback that operates during fate specification in these cells.

We wish to thank Richard Ruiz and Xinlan Zhou for technical assistance, Shoshana Posy for expert help on building phylogenetic trees, Luke Ward and Geraldine Seydoux for contributions to this work, Dan Shaye for comments on the manuscript, and Barth Grant and members of the Greenwald and Hobert laboratories, particularly Iskra Katic, Dan Shaye, Claire Benard and Oliver Hobert, for much useful discussion. Some nematode strains used in this work were provided by the Caenorhabditis Genetics Center, which is funded by the National Institutes of Health (NIH) National Center for Research Resources. N.d.S. is a Postdoctoral Associate and I.G. an Investigator of the Howard Hughes Medical Institute.

References

Bettinger, J. C., Lee, K. and Rougvie, A. E. (1996). Stage-specific accumulation of the terminal differentiation factor LIN-29 during Caenorhabditis elegans development. *Development* **122**, 2517-2527.

Bonifacino, J. S. and Rojas, R. (2006). Retrograde transport from endosomes to the trans-Golgi network. *Nat. Rev. Mol. Cell Biol.* **7**, 568-579.

Brown, P. S., Wang, E., Aroeti, B., Chapin, S. J., Mostov, K. E. and Dunn, K. W. (2000). Definition of distinct compartments in polarized Madin-Darby canine kidney (MDCK) cells for membrane-volume sorting, polarized sorting and apical recycling. *Traffic* **1**, 124-140.

Burdine, R. D., Branda, C. S. and Stern, M. J. (1998). EGL-17(FGF) expression coordinates the attraction of the migrating sex myoblasts with vulval induction in C. elegans. *Development* **125**, 1083-1093.

Burke, P., Schooler, K. and Wiley, H. S. (2001). Regulation of epidermal growth factor receptor signaling by endocytosis and intracellular trafficking. *Mol. Biol. Cell* **12**, 1897-1910.

Casanova, J. E., Wang, X., Kumar, R., Bhartur, S. G., Navarre, J., Woodrum, J.

E., Altschuler, Y., Ray, G. S. and Goldenring, J. R. (1999). Association of Rab25 and Rab11a with the apical recycling system of polarized Madin-Darby canine kidney cells. *Mol. Biol. Cell* **10**, 47-61.
Castermans, D., Wilquet, V., Parthoens, E., Huysmans, C., Steyaert, J., Swinnen, L., Fryns, J. P., Van de Ven, W. and Devriendt, K. (2003). The neurobeachin gene is disrupted by a translocation in a patient with idiopathic autism. *J. Med. Genet.* **40**, 352-356.
Chen, C. C., Schweinsberg, P. J., Vashist, S., Mareiniss, D. P., Lambie, E. J. and Grant, B. D. (2006). RAB-10 is required for endocytic recycling in the Caenorhabditis elegans intestine. *Mol. Biol. Cell* **17**, 1286-1297.
Chen, N. and Greenwald, I. (2004). The lateral signal for LIN-12/Notch in C. elegans vulval development comprises redundant secreted and transmembrane DSL proteins. *Dev. Cell* **6**, 183-192.
Chenna, R., Sugawara, H., Koike, T., Lopez, R., Gibson, T. J., Higgins, D. G. and Thompson, J. D. (2003). Multiple sequence alignment with the Clustal series of programs. *Nucleic Acids Res.* **31**, 3497-3500.
Chow, K. L., Hall, D. H. and Emmons, S. W. (1995). The mab-21 gene of Caenorhabditis elegans encodes a novel protein required for choice of alternate cell fates. *Development* **121**, 3615-3626.
Clokey, G. V. and Jacobson, L. A. (1986). The autofluorescent "lipofuscin granules" in the intestinal cells of Caenorhabditis elegans are secondary lysosomes. *Mech. Ageing Dev.* **35**, 79-94.
Dyomin, V. G., Chaganti, S. R., Dyomina, K., Palanisamy, N., Murty, V. V., Dalla-Favera, R. and Chaganti, R. S. (2002). BCL8 is a novel, evolutionarily conserved human gene family encoding proteins with presumptive protein kinase A anchoring function. *Genomics* **80**, 158-165.
Fares, H. and Grant, B. (2002). Deciphering endocytosis in Caenorhabditis elegans. *Traffic* **3**, 11-19.
Finley, K. D., Edeen, P. T., Cumming, R. C., Mardahl-Dumesnil, M. D., Taylor, B. J., Rodriguez, M. H., Hwang, C. E., Benedetti, M. and McKeown, M. (2003). blue cheese mutations define a novel, conserved gene involved in progressive neural degeneration. *J. Neurosci.* **23**, 1254-1264.
Gebauer, D., Li, J., Jogl, G., Shen, Y., Myszka, D. G. and Tong, L. (2004). Crystal structure of the PH-BEACH domains of human LRBA/BGL. *Biochemistry* **43**, 14873-14880.
Gonzalez-Gaitan, M. (2003). Signal dispersal and transduction through the endocytic pathway. *Nat. Rev. Mol. Cell Biol.* **4**, 213-224.
Grant, B., Zhang, Y., Paupard, M. C., Lin, S. X., Hall, D. H. and Hirsh, D. (2001). Evidence that RME-1, a conserved C. elegans EH-domain protein, functions in endocytic recycling. *Nat. Cell Biol.* **3**, 573-579.
Greenwald, I. (2005). LIN-12/Notch signaling in C. elegans. In *WormBook* (ed. The *C. elegans* Research Community), doi/10.1895/wormbook.1.10.1, http:/www.wormbook.org.
Greenwald, I. and Seydoux, G. (1990). Analysis of gain-of-function mutations of the lin-12 gene of Caenorhabditis elegans. *Nature* **346**, 197-199.
Greenwald, I. S., Sternberg, P. W. and Horvitz, H. R. (1983). The lin-12 locus specifies cell fates in Caenorhabditis elegans. *Cell* **34**, 435-444.
Han, J. D., Baker, N. E. and Rubin, C. S. (1997). Molecular characterization of a novel A kinase anchor protein from Drosophila melanogaster. *J. Biol. Chem.* **272**, 26611-26619.
Hermann, G. J., Schroeder, L. K., Hieb, C. A., Kershner, A. M., Rabbitts, B. M., Fonarev, P., Grant, B. D. and Priess, J. R. (2005). Genetic analysis of lysosomal trafficking in Caenorhabditis elegans. *Mol. Biol. Cell* **16**, 3273-3288.
Herz, H. M., Chen, Z., Scherr, H., Lackey, M., Bolduc, C. and Bergmann, A. (2006). vps25 mosaics display non-autonomous cell survival and overgrowth, and autonomous apoptosis. *Development* **133**, 1871-1880.
Hoekstra, D., Tyteca, D. and van IJzendoorn, S. C. (2004). The subapical compartment: a traffic center in membrane polarity development. *J. Cell Sci.* **117**, 2183-2192.
Hubbard, E. J., Wu, G., Kitajewski, J. and Greenwald, I. (1997). sel-10, a negative regulator of lin-12 activity in Caenorhabditis elegans, encodes a member of the CDC4 family of proteins. *Genes Dev.* **11**, 3182-3193.
Inoue, T., Sherwood, D. R., Aspock, G., Butler, J. A., Gupta, B. P., Kirouac, M., Wang, M., Lee, P. Y., Kramer, J. M., Hope, I. et al. (2002). Gene expression markers for Caenorhabditis elegans vulval cells. *Gene Expr. Patterns* **2**, 235-241.
Jogl, G., Shen, Y., Gebauer, D., Li, J., Wiegmann, K., Kashkar, H., Kronke, M. and Tong, L. (2002). Crystal structure of the BEACH domain reveals an unusual fold and extensive association with a novel PH domain. *EMBO J.* **21**, 4785-4795.
Kaech, S. M., Whitfield, C. W. and Kim, S. K. (1998). The LIN-2/LIN-7/LIN-10 complex mediates basolateral membrane localization of the C. elegans EGF receptor LET-23 in vulval epithelial cells. *Cell* **94**, 761-771.
Kim, S. K. (1997). Polarized signaling: basolateral receptor localization in epithelial cells by PDZ-containing proteins. *Curr. Opin. Cell Biol.* **9**, 853-859.
Le Roy, C. and Wrana, J. L. (2005). Clathrin- and non-clathrin-mediated endocytic regulation of cell signalling. *Nat. Rev. Mol. Cell Biol.* **6**, 112-126.
Levitan, D. and Greenwald, I. (1998). LIN-12 protein expression and localization during vulval development in C. elegans. *Development* **125**, 3101-3109.
Miaczynska, M., Pelkmans, L. and Zerial, M. (2004). Not just a sink: endosomes in control of signal transduction. *Curr. Opin. Cell Biol.* **16**, 400-406.
Moberg, K. H., Schelble, S., Burdick, S. K. and Hariharan, I. K. (2005). Mutations in erupted, the Drosophila ortholog of mammalian tumor susceptibility gene 101, elicit non-cell-autonomous overgrowth. *Dev. Cell* **9**, 699-710.
Mostov, K., Su, T. and ter Beest, M. (2003). Polarized epithelial membrane traffic: conservation and plasticity. *Nat. Cell Biol.* **5**, 287-293.
Nagle, D. L., Karim, M. A., Woolf, E. A., Holmgren, L., Bork, P., Misumi, D. J., McGrail, S. H., Dussault, B. J., Jr, Perou, C. M., Boissy, R. E. et al. (1996). Identification and mutation analysis of the complete gene for Chediak-Higashi syndrome. *Nat. Genet.* **14**, 307-311.
Notredame, C., Higgins, D. G. and Heringa, J. (2000). T-Coffee: a novel method for fast and accurate multiple sequence alignment. *J. Mol. Biol.* **302**, 205-217.
Page, R. D. (1996). TreeView: an application to display phylogenetic trees on personal computers. *Comp. Appl. Biosci.* **12**, 357-358.
Sato, M., Sato, K., Fonarev, P., Huang, C. J., Liou, W. and Grant, B. D. (2005). Caenorhabditis elegans RME-6 is a novel regulator of RAB-5 at the clathrin-coated pit. *Nat. Cell Biol.* **7**, 559-569.
Savelyeva, L., Sagulenko, E., Schmitt, J. G. and Schwab, M. (2006). The neurobeachin gene spans the common fragile site FRA13A. *Hum. Genet.* **118**, 551-558.
Schreiber, S. L., Preiss, A., Nagel, A. C., Wech, I. and Maier, D. (2002). Genetic screen for modifiers of the rough eye phenotype resulting from overexpression of the Notch antagonist hairless in Drosophila. *Genesis* **33**, 141-152.
Shamloula, H. K., Mbogho, M. P., Pimentel, A. C., Chrzanowska-Lightowlers, Z. M., Hyatt, V., Okano, H. and Venkatesh, T. R. (2002). rugose (rg), a Drosophila A kinase anchor protein, is required for retinal pattern formation and interacts genetically with multiple signaling pathways. *Genetics* **161**, 693-710.
Shaye, D. D. and Greenwald, I. (2002). Endocytosis-mediated downregulation of LIN-12/Notch upon Ras activation in Caenorhabditis elegans. *Nature* **420**, 686-690.
Shaye, D. D. and Greenwald, I. (2005). LIN-12/Notch trafficking and regulation of DSL ligand activity during vulval induction in Caenorhabditis elegans. *Development* **132**, 5081-5092.
Simonsen, A., Birkeland, H. C., Gillooly, D. J., Mizushima, N., Kuma, A., Yoshimori, T., Slagsvold, T., Brech, A. and Stenmark, H. (2004). Alfy, a novel FYVE-domain-containing protein associated with protein granules and autophagic membranes. *J. Cell Sci.* **117**, 4239-4251.
Sondek, J., Bohm, A., Lambright, D. G., Hamm, H. E. and Sigler, P. B. (1996). Crystal structure of a G-protein beta gamma dimer at 2.1A resolution. [erratum appears in *Nature* (1996) **379**, 847] *Nature* **379**, 369-374.
Sorkin, A. and Waters, C. M. (1993). Endocytosis of growth factor receptors. *BioEssays* **15**, 375-382.
Stahl, P. D. and Barbieri, M. A. (2002). Multivesicular bodies and multivesicular endosomes: the "ins and outs" of endosomal traffic. *Sci. Stke* **2002**, PE32.
Stetak, A., Frohli Hoier, E., Croce, A., Cassata, G., Di Fiore, P. and Hajnal, A. (2006). Cell fate-specific regulation of EGF receptor trafficking during Caenorhabditis elegans vulval development. *EMBO J.* **25**, 2347-2357.
Struhl, G., Fitzgerald, K. and Greenwald, I. (1993). Intrinsic activity of the Lin-12 and Notch intracellular domains in vivo. *Cell* **74**, 331-345.
Su, Y., Balice-Gordon, R. J., Hess, D. M., Landsman, D. S., Minarcik, J., Golden, J., Hurwitz, I., Liebhaber, S. A. and Cooke, N. E. (2004). Neurobeachin is essential for neuromuscular synaptic transmission. *J. Neurosci.* **24**, 3627-3636.
Sundaram, M. V. (2006). RTK/Ras/MAPK signaling. In *WormBook* (ed. The *C. elegans* Research Community), doi/10.1895/ wormbook.1.80.1, http://www.wormbook.org.
Swofford, D. L. (2003). *PAUP: Phylogenetic Analysis Using Parsimony and Other Methods*. Sunderland, MA: Sinauer Associates.
Thompson, B. J., Mathieu, J., Sung, H. H., Loeser, E., Rorth, P. and Cohen, S. M. (2005). Tumor suppressor properties of the ESCRT-II complex component Vps25 in Drosophila. *Dev. Cell* **9**, 711-720.
Timmons, L., Court, D. L. and Fire, A. (2001). Ingestion of bacterially expressed dsRNAs can produce specific and potent genetic interference in Caenorhabditis elegans. *Gene* **263**, 103-112.
Urano, F., Calfon, M., Yoneda, T., Yun, C., Kiraly, M., Clark, S. G. and Ron, D. (2002). A survival pathway for Caenorhabditis elegans with a blocked unfolded protein response. *J. Cell Biol.* **158**, 639-646.
Vaccari, T. and Bilder, D. (2005). The Drosophila tumor suppressor vps25 prevents nonautonomous overproliferation by regulating notch trafficking. *Dev. Cell* **9**, 687-698.
Vieira, A. V., Lamaze, C. and Schmid, S. L. (1996). Control of EGF receptor signaling by clathrin-mediated endocytosis. *Science* **274**, 2086-2089.
Wall, M. A., Coleman, D. E., Lee, E., Iniguez-Lluhi, J. A., Posner, B. A., Gilman, A. G. and Sprang, S. R. (1995). The structure of the G protein heterotrimer Gi alpha 1 beta 1 gamma 2. *Cell* **83**, 1047-1058.
Wang, E., Brown, P. S., Aroeti, B., Chapin, S. J., Mostov, K. E. and Dunn, K. W. (2000a). Apical and basolateral endocytic pathways of MDCK cells meet in acidic common endosomes distinct from a nearly-neutral apical recycling endosome. *Traffic* **1**, 480-493.
Wang, J. W., Howson, J., Haller, E. and Kerr, W. G. (2001). Identification of a

novel lipopolysaccharide-inducible gene with key features of both A kinase anchor proteins and chs1/beige proteins. *J. Immunol.* **166**, 4586-4595.
Wang, J. W., Gamsby, J. J., Highfill, S. L., Mora, L. B., Bloom, G. C., Yeatman, T. J., Pan, T. C., Ramne, A. L., Chodosh, L. A., Cress, W. D. et al. (2004). Deregulated expression of LRBA facilitates cancer cell growth. *Oncogene* **23**, 4089-4097.
Wang, X., Herberg, F. W., Laue, M. M., Wullner, C., Hu, B., Petrasch-Parwez, E. and Kilimann, M. W. (2000b). Neurobeachin: a protein kinase A-anchoring, beige/Chediak-higashi protein homolog implicated in neuronal membrane traffic. *J. Neurosci.* **20**, 8551-8565.
Wech, I. and Nagel, A. C. (2005). Mutations in rugose promote cell type-specific apoptosis in the Drosophila eye. *Cell Death Differ.* **12**, 145-152.
Wen, C. and Greenwald, I. (1999). p24 proteins and quality control of LIN-12 and GLP-1 trafficking in Caenorhabditis elegans. *J. Cell Biol.* **145**, 1165-1175.
Whitfield, C. W., Benard, C., Barnes, T., Hekimi, S. and Kim, S. K. (1999). Basolateral localization of the Caenorhabditis elegans epidermal growth factor receptor in epithelial cells by the PDZ protein LIN-10. *Mol. Biol. Cell* **10**, 2087-2100.
Wilkinson, H. A., Fitzgerald, K. and Greenwald, I. (1994). Reciprocal changes in expression of the receptor lin-12 and its ligand lag-2 prior to commitment in a C. elegans cell fate decision. *Cell* **79**, 1187-1198.
Yoo, A. S. and Greenwald, I. (2005). LIN-12/Notch activation leads to microRNA-mediated down-regulation of Vav in C. elegans. *Science* **310**, 1330-1333.
Yoo, A. S., Bais, C. and Greenwald, I. (2004). Crosstalk between the EGFR and LIN-12/Notch pathways in C. elegans vulval development. *Science* **303**, 663-666.
Zerial, M. and McBride, H. (2001). Rab proteins as membrane organizers. [erratum appears in *Nat. Rev. Mol. Cell Biol.* (2001) **2**, 216] *Nat. Rev. Mol. Cell Biol.* **2**, 107-117.